Substructures in lens galaxies: PG1115+080 and B1555+375, two fold configurations

Marco Miranda and Philippe Jetzer

Institute for Theoretical Physics, University of Zürich, Winterthurerstrasse 190, CH-8057 Zürich, Switzerland

Abstract

We study the anomalous flux ratio which is observed in some four-image lens systems, where the source lies close to a fold caustic. In this case two of the images are close to the critical curve and their flux ratio should be equal to unity, instead in several cases the observed value differs significantly. The most plausible solution is to invoke the presence of substructures, as for instance predicted by the Cold Dark Matter scenario, located near the two images. In particular, we analyze the two fold lens systems PG1115+080 and B1555+375, for which there are not yet satisfactory models which explain the observed anomalous flux ratios. We add to a smooth lens model, which reproduces well the positions of the images but not the anomalous fluxes, one or two substructures described as singular isothermal spheres. For PG1115+080 we consider a smooth model with the influence of the group of galaxies described by a SIS and a substructure with mass $\sim 10^5\ M_\odot$ as well as a smooth model with an external shear and one substructure with mass $\sim 10^8\ M_\odot$. For B1555+375 either a strong external shear or two substructures with mass $\sim 10^7\ M_\odot$ reproduce the data quite well.

Key words: cosmology: theory – dark matter – gravitational lensing – galaxies: haloes – substructures

1 Introduction

The standard lens models, although reproduce in general the relative positions of the images quite accurately, often have difficulties explaining the relative fluxes of multiply-imaged sources. Several possible explanations have been considered in the literature, the most plausible being that the lensing potential of real galaxies are not fully described by the simple lens models used to compute the lens characteristics. The most often invoked solution is to consider additional small-scale structures, which if located near the images can modify

significantly the observed flux ratio between different images, in particular the so-called cusp or fold relations.

The presence of substructures is naturally expected within the Cold Dark Matter (CDM) model, which has been successful in explaining a large variety of observational results like the large scale structure of galaxies on scales larger than 1 Mpc or the fluctuations of the CMB (Spergel et al 2003). However, one of the predictions of this scenario is a distribution of matter, with a large number of small-mass compact dark matter (DM subhalos) halos, both within virialized regions of larger halos (Moore et al. 1999, Klypin et al. 1999) and in the field (DM extragalactic halos, Metcalf 2005). At the same time, the observed number of dwarf galaxy satellites in the Local Group is more than an order of magnitude smaller than expected. Many theoretical studies suggest models to reduce the abundance of substructure or to suppress star formation in small clumps via astrophysical mechanisms (as feedback), making them dark (Bullock, Kravtosov & Weinberg 2000, Kravtsov et al. 2004, Moore et al. 2006). Anyway, if the CDM paradigm is correct, we expect $\sim 10 - 15\%$ of the mass of a present-day galactic halo ($\sim 10^{12} M_{\odot}$) within the virial radius to be in substructures with mass $\geq 10^{7} M_{\odot}$. Thus in the CDM model anomalous flux ratios should be common.

At present, the only way to detect these subclumps is through gravitational lensing, which is directly sensitive to the mass. This is because substructures (like globular clusters, gas clouds or satellite galaxies) can strongly modify the fluxes of lensed images relative to those predicted by smooth lens models. Even a clump as small as a star can perturb the image of small sources (~ 100 AU), but in this case we would see a microlensing effect such as variability in the image brightness with a time scale of order months. Some authors tried to fit systems (for example the radio system B1422+231) with anomalous flux ratios using smooth lens and multipole models: although it seems necessary to investigate further whether the multipoles can fit the lens configurations, these methods are not exhaustive (Evans & Witt 2003, Kochanek & Dalal 2004, Congdon & Keeton 2005) and it is not yet possible to conclude that the multipole approach can explain the anomalous flux ratios. Indeed, Kochanek & Dalal 2004 showed that the flux anomaly distributions display the characteristic demagnifications of the brightest saddle point relative to the other images expected for low optical depth substructure, which they conclude cannot be mimicked by problems in the "macro" models for the gravitational potential of the lens galaxy. Mao & Schneider (1998), Keeton (2001), Metcalf & Madau (2001), Bradač et al. (2002), Dobler &Keeton (2006) noted that a simple way of solving the puzzle was to put a satellite near the images, and they found that this could explain the anomaly in B1422+231.

Generally the flux ratios between the images do not depend on wavelength since they are independent of the intrinsic flux and variability of the source

(Keeton et al. 1997, Mao & Schneider 1998, Keeton 2001, Metcalf & Zhao 2002). Such discrepancies would probably be due to sub-lensing or microlensing effects. On the other hand when modeling a multiple QSO lens system, one can either include or disregard the flux ratios of the images. As pointed out by Chang & Refsdal (1979) (and in the following by several authors, as for instance Metcalf 2005, Keeton et al. 2005, Mortonson et al. 2005) we have to pay attention to the fact that the projected (on the lens plane) sizes of the optical continuum emitting regions of QSOs are expected to be of the same order as the Einstein radius of a star in the lens galaxy ($\sim$ 100AU), so that the optical magnitudes may well be affected by gravitational microlensing (see Metcalf et al. 2004, Mortonson et al. 2005, and references therein), even if averaged over long periods of time. The radio and mid-IR regions, when projected on the lens plane, are typically of the order of 10 pc and change in their magnification should be dominated by larger scales than stars (Metcalf 2005, Chiba et al. 2005). If the lens galaxies contain substructures with an Einstein radius comparable or greater than the projected size of the radio component (corresponding for the substructure to masses $\geq 10^8 M_\odot$) we should see image splitting and distortions if they lie close enough to the images (see section 3.2, Wambsganss & Paczyński 1994, Mao & Schneider 1998), which have not yet been detected (this might be the case for B0128+437, Biggs et al. 2004).

The existence of anomalous fluxes in many lens systems has been known since some time. The substructure lensing effects have been studied by considering single substructures (Mao & Schneider 1998, Metcalf & Madau 2001), by assuming a statistically distributed sample of substructures (Chiba 2002, Chen et al. 2003, Keeton et al. 2005) or by simulations (Amara et al. 2006, Macciò et al. 2005). [1] An explanation by lensing of substructures for the anomalous flux ratio for the PG1115+080 system has already been considered (Chiba 2002, Dalal & Kochanek 2002, Chen et al. 2003, Kochanek & Dalal 2004, Keeton, Gaudi, Petters 2005), however, mainly within a statistical treatment to determine whether a plausible collection of mass clumps could explain the strange flux ratio. As pointed out by Chiba (2002), even if it seems difficult to reproduce anomalous flux ratios with CDM subhalos, he concluded that the main role in reproducing the observed flux ratio is played by the one satellite which is located in the vicinity of an image (either A1 or A2 in PG1115+80).

In this paper we analyze in detail the lens system by adding one or two subclumps nearby one of the images and by solving the lens equation. In section 2 we review the main observation and analysis done so far on the two lens systems PG1115+080 and B1555+375. In section 3 we briefly recall the relevant formalism for gravitational lensing and how we proceed when we consider a lens model with a perturbation induced by one or more substructures. Assuming a SIS model for the substructures we can then get an estimate on their

[1] These works deal with violations of the cusp relation.

position and Einstein radius (or mass) such as to modify the flux of the image pair near the critical curve due to a source located close to a fold. In section 4 we present the numerical simulations and fits to the two considered lens systems. We conclude with a short summary and discussion of our results in section 5.

2 About PG1115+080 and B1555+375

PG1115+080 is the second gravitationally lensed quasar which was discovered (Weymann et al. 1980, Impey et al. 1998 and references therein). The source is at redshift $z_s = 1.722$ and the lens galaxy at $z_l = 0.310$. It is an optically selected, radio-quiet quasar. Hege et al. (1981) first resolved the four quasar images (a close pair A2/A1, B and C), confirming the early model of Young et al. (1981) that the lens is a five-images system, one image being hidden by the core of the lens galaxy.

Young et al. (1981) noted that the lens galaxy seems to be part of a small group centered to the southwest of the lens, with a velocity dispersion of approximately 270 ± 70 km s^{-1} based only on four galaxy redshifts (Tonry 1998 also confirmed the group velocity dispersion by using five galaxies and getting a value of 326 kms^{-1}). The group is an essential component of any model to successfully fit the lens constraints (Keeton et al. 1997; Schechter et al. 1997). Also two time delays between the images were determined by Schechter et al. (1997) and confirmed by Barkana (1997). Their results were analyzed by Keeton & Kochanek (1997) and Courbin et al. (1997) by assuming power law mass distributions and leading to a value of $H_0 = 53^{+15}_{-7}$ km s^{-1} Mpc^{-1}, with comparable contributions to the uncertainties both from the time delay measurements and the models. Recently, Read et al. 2007, assuming a non parametric mass distribution, found $H_0 = 64^{+8}_{-9}$ km s^{-1} Mpc^{-1} consistent with the currently accepted value of about 70 km s^{-1} Mpc^{-1}.

We take the data for the PG1115+080 system from Impey et al. (1998) (their Fig.1 and Tables 1 and 2) who presented a near-infrared observation of the PG1115+080 system obtained with the Hubble Space Telescope (HST) NICMOS camera. The flux ratio of the close pair of images (A1 and A2, see Fig. 1) is approximately 0.67 and showed little variation with wavelength from the multiple wavelength observations by Impey et al. (1998) [2]. Simple lens models require instead an A2/A1 flux ratio close to 1, because the images are symmetrically arranged near a fold caustic. There is no smooth lens model that can explain this anomalous flux: while each of such models can differ in

[2] Pooley et al. (2006), however, report that there has been some variation also in the optical.

complexity or in parameterization, the observed discrepancy in the flux ratio, compared with the expected universal relations for a cusp or fold singularity, suggests that it is an intrinsic difficulty for smooth lens models, not associated with a particular choice of the parameters (Yoo et al. 2005).

Recently, Chiba et al. (2005) analyzed observations of the PG1115+080 system done in the mid-infrared band and found a flux ratio A2/A1 of 0.93 for the close pair, which is virtually consistent with smooth lens models but clearly inconsistent with the optical fluxes. The observations indicated that the measured mid-infrared flux originate from a hot dust torus around a QSO nucleus. Based on the size estimate of the dust torus, they placed limits on the mass of the substructure causing the optical flux anomaly [3]. For a substructure modeled as a SIS the subclumps should have a mass of at most $2.2 \times 10^4 M_\odot$ inside a radius of 100pc to prevent anomalies in the mid-infrared band. However, it has to be pointed out that this latter result is based on several assumptions and few observations (Minezaki et al. 2004), so that the given value may be subject to substantial modifications. Indeed, if the size of the cooler dust torus causing the mid-infrared flux is underestimated then the above limit gets increased. Furthermore, Pooley et al. 2006 analyzed the system using recent X-ray observations, which show also a strong anomalous flux ratio. They do not exclude the microlensing hypothesis in order to explain the anomaly in the X-ray band, nonetheless they conclude that the optical emission region should be much larger (by a factor $\approx 10 - 100$) than predicted by a simple thin accretion disk model. Within this model the source size should be $R_s \approx 10^{15} cm$ (e.g. Wambsganss, Schneider, & Paczyński 1990; Rauch & Blandford 1991; Wyithe et al. 2000). Therefore, if it is 10-100 bigger, $R_s \approx 0.01 - 0.1$ pc, the effect of stellar microlensing could be ruled out (Metcalf 2005).

An interesting quadruply imaged lens system is B1555+375 with a maximum separation of only 0.42 arcsec, which was discovered some years ago (Marlow et al. 1999). It has an anomalous flux ratio in the radio: the system was observed at 8,4 GHz at VLA and with MERLIN 5 GHz snapshot observations. There are only few observations in the optical and near-infrared band. Marlow et al. (1999) considered a model for B1555+375, which describes well the positions of the images but fails to reproduce accurately the flux ratio between the two images near the fold critical point (labeled by A and B, see Fig.3). The observed ratio is about B/A ~ 0.57. This anomaly has also been discussed by Keeton et al. (2005) and Dobler & Keeton (2006). As the redshifts of lens and source have not yet been measured we will adopt the same values as used by

[3] They also considered for this system the microlensing hypothesis and estimated the time variability of the images flux in the mid-infrared band, which turned out to be rather long (more than a decade). This estimate is consistent with the fact that the optical flux ratio has remained unchanged over the past decade. It is thus clearly not yet possible to assess the microlensing hypothesis.

Image	H	I	V
	mag	mag	mag
A1	15.75±0.02	16.12	16.90
A2	16.23±0.03	16.51	17.35
B	17.68±0.04	18.08	18.87
C	17.23±0.03	17.58	18.37
Lens	16.57±0.10	18.40	-

Table 1
Photometric data in 3 bands for the four images of PG1115+080, from Impey et al. (1998).

Marlow et al. (1999): $z_l = 0.5$ and $z_s = 1.5$.

3 Analytical treatment

We briefly recall the general expressions for the gravitational lensing and refer, e.g., to the book by Schneider et al. (1992) (which we will denote afterwards with SEF) and the review by Kochanek (2004). The lens equation is

$$\vec{\beta} = \vec{\theta} - \vec{\alpha}(\vec{\theta}) \ , \tag{1}$$

where $\vec{\beta}(\vec{\theta})$ is the source position and $\vec{\theta}$ the image position. $\vec{\alpha}(\vec{\theta})$ is the deflection angle, which depends on $\kappa(\vec{\theta})$ the dimensionless surface mass density or convergence in units of the critical surface mass density $\Sigma_{\rm crit}$, defined as

$$\Sigma_{\rm crit} = \frac{c^2}{4\pi G}\frac{D_S}{D_L D_{LS}}, \tag{2}$$

where D_S, D_L, D_{LS} are the angular diameter distances between observer and source, observer and lens, source and lens, respectively.

3.1 Lens Mapping

In the vicinity of an arbitrary point, the lens mapping can be described by its Jacobian matrix $\mathcal{A}$:

$$\mathcal{A} = \frac{\partial\vec{\beta}}{\partial\vec{\theta}} = \left(\delta_{ij} - \frac{\partial\alpha_i(\vec{\theta})}{\partial\theta_j}\right) = \left(\delta_{ij} - \frac{\partial^2\psi(\vec{\theta})}{\partial\theta_i\partial\theta_j}\right). \tag{3}$$

Here we made use of the fact (see SEF), that the deflection angle can be expressed as the gradient of an effective two-dimensional scalar potential ψ: $\vec{\alpha} = \vec{\nabla}_\theta \psi$, which carries information on the Newtonian potential of the lens. The magnification is defined as the ratio between the solid angles of the image and the source (since the surface brightness is conserved) and is given by the inverse of the determinant of the Jacobian $\mathcal{A}$

$$\mu = \frac{1}{\det \mathcal{A}}. \tag{4}$$

The Laplacian of the effective potential ψ is twice the convergence:

$$\psi_{11} + \psi_{22} = 2\kappa = \text{tr } \psi_{ij}. \tag{5}$$

With the definitions for the components of the external shear γ:

$$\gamma_1(\vec{\theta}) = \frac{1}{2}(\psi_{11} - \psi_{22}) = \gamma(\vec{\theta}) \cos[2\varphi(\vec{\theta})] \tag{6}$$

and

$$\gamma_2(\vec{\theta}) = \psi_{12} = \psi_{21} = \gamma(\vec{\theta}) \sin[2\varphi(\vec{\theta})] \tag{7}$$

(where the angle φ gives the direction of the shear) the Jacobian matrix can be written as

$$\mathcal{A} = \begin{pmatrix} 1 - \kappa - \gamma_1 & -\gamma_2 \\ -\gamma_2 & 1 - \kappa + \gamma_1 \end{pmatrix} \tag{8}$$

$$= (1 - \kappa) \begin{pmatrix} 1 & 0 \\ 0 & 1 \end{pmatrix} - \gamma \begin{pmatrix} \cos 2\varphi & \sin 2\varphi \\ \sin 2\varphi & -\cos 2\varphi \end{pmatrix}, \tag{9}$$

where $\gamma = \sqrt{\gamma_1^2 + \gamma_2^2}$. With eq.(8) the magnification can be expressed as a function of the convergence κ and the shear γ at the image point:

$$\mu = (\det \mathcal{A})^{-1} = \frac{1}{(1 - \kappa)^2 - \gamma^2}. \tag{10}$$

Locations at which $\det A = 0$ have formally infinite magnification are the critical curves in the lens plane. The corresponding locations in the source plane are the caustics. For spherically symmetric mass distributions the critical

curves are circles, whereas for elliptical lenses or spherically symmetric lenses with external shear, the caustics can have cusps and folds.

Near a fold the lens equation can be reduced to a one-dimensional model and a Taylor expansion can be performed (see SEF, Kochanek 2004), for which we get

$$\beta - \beta_0 = \frac{\partial \beta}{\partial \theta}(\theta - \theta_0) + \frac{1}{2}\frac{\partial^2 \beta}{\partial \theta^2}(\theta - \theta_0)^2, \tag{11}$$

i.e.

$$\beta = \theta\,(1 - \psi'') - \frac{1}{2}\psi'''\theta^2 \rightarrow -\frac{1}{2}\psi'''\theta^2 \tag{12}$$

and inverse magnification

$$\mu^{-1} = (1 - \psi'') - \psi'''\theta \rightarrow -\psi'''\theta. \tag{13}$$

We choose the coordinate system such that there is a critical line at $\theta = 0$ (i.e. $1 - \psi'' = 0$) and the primes denote derivatives with respect to θ. These equations are easily solved and one finds that the two images are at $\theta_\pm = \pm(-2\beta/\psi''')^{1/2}$ with inverse magnifications $\mu_\pm^{-1} = \mp(-2\beta\psi''')^{1/2}$ that are equal in magnitude but with opposite sign. Hence, if the assumptions for the Taylor expansion hold, the images merging at a fold should have identical fluxes. Using gravity to produce anomalous flux ratios requires terms in the potential with a length scale comparable to the separation of the images to significantly violate the rule that they should have similar fluxes.

3.2 Perturbing the system

Let's consider a general lens system configuration for which we know flux ratios and image positions and we assume to be able to reproduce with a smooth lens model, such as a singular isothermal ellipsoid (SIE), the main features of the lens, besides the anomalous flux ratio. Adding an external potential term in the lens equation and correspondingly in the Jacobian matrix such as induced by singular isothermal sphere (SIS) substructures perturb the system. Keeton (2001) analyzing the system B1422+231 (cusp case), could put limits on the subclump mass range by considering the different effects they would induce on optical and radio bands. For the same system Bradač et al. (2002) suggests a way to estimate the minimum value for the convergence k in order to get agreement with the observed flux ratios.

Here we constrain the mass and the position of a substructure by considering its effects on the flux of the images. At each image position the perturbed Jacobian matrix can be written as

$$\mathcal{A} = \begin{pmatrix} 1 - \kappa_1 - \tilde{\gamma}_1 & -\tilde{\gamma}_2 \\ -\tilde{\gamma}_2 & 1 - \kappa_1 - \tilde{\gamma}_1 \end{pmatrix}, \tag{14}$$

where $\kappa_1 = (\kappa + \Delta\kappa), \tilde{\gamma}_1 = (\gamma_1 + \Delta\gamma_1), \tilde{\gamma}_2 = (\gamma_2 + \Delta\gamma_2)$ and $\Delta\kappa, \Delta\gamma_1$ and $\Delta\gamma_2$ are the perturbations induced by a substructure.

If the substructure is modeled by a SIS, it is possible to express the shear components as a function of $\Delta\kappa$ (this is true for models that have radial symmetry, Kormann et al. (1994)): $\Delta\gamma_1 = \Delta\kappa cos\theta_{sis}$ and $\Delta\gamma_2 = \Delta\kappa sin\theta_{sis}$, where

$$\Delta\kappa = \frac{R_{sis}}{2\sqrt{(x_{sis} - x_P)^2 + (y_{sis} - y_P)^2}}. \tag{15}$$

(x_{sis}, y_{sis}) is the position of the substructure and (x_P, y_P) is the considered image position. R_{sis} is the Einstein radius of the substructure, which depends on its mass and the distances (or redshifts) to the lens and the source, the latter ones being known quantities. The θ_{sis} is given through the relation $tg\theta_{sis} = (x_{sis} - x_P)/(y_{sis} - y_P)$ and it is the angle between the SIS and the considered image position (x_P, y_P). We first consider a model with one additional substructure located at the same distance as the lens. Its mass and position have to be determined such that the substructure does not significantly (within the observational errors) modify the positions of all the images as well as the fluxes of the images which lie far from the two ones near the fold critical point. These requirements clearly put constraints on the mass and position of the substructure.

For the determination of the magnification of an image the additional terms due to the substructure depend only on the position (x_{sis}, y_{sis}) and the mass (Einstein radius R_{sis}) of the subclump, thus we have 3 unknown quantities (see Appendix). We consider only three images, thus getting a system with three equations for three unknown quantities, and assume that the 4th image is far enough such as not to be perturbed by the substructure. We then verify a posteriori that the found solution satisfies this latter assumption within the measurement errors. It turns out indeed to be the case, as the subclump is located far from the 4th image, which is chosen as being the most distant one from the two near the fold. The system of equations is non-linear, so that the solution is not unique (see Appendix A). However, some solutions have to be discarded as being not physical (imaginary values or a negative

Einstein radius). All acceptable solutions are taken as input parameters for the simulations, as will be discussed in the next Section (see also Fig. 1).

Note that the substructure could produce further multiple images of the original one. In our case, where we model the substructures as SIS, necessary and sufficient condition for multiple images formation is that the Einstein radius (of the subclump) θ_{Esub} has to be greater than half of θ_I, the distance of the image from the subclump ($\theta_{Esub} \geq (1/2)\theta_I$) (Narayan & Schneider 1990). In Tables 4 and 7 we give the positions of the substructures and of the images for the two considered lens systems as obtained from the simulations as discussed in the next section. From these data one easily verifies that the Einstein radius of the substructures, as given in Tables 2 and 6, do not satisfy the above condition, thus ruling out the formation of further images. As noticed by Keeton (2003), for SIS subclumps positive-parity images get always brighter, whereas negative-parity images get fainter. In our case for PG1115+080 (B1555+375) A1 (A) is the positive-parity image and A2 (B) the negative-parity one.

4 Numerical simulations

In this section we present our simulations and results. We use the gravlens code developed by Keeton (2001) [4], modeling the main galaxy acting as lens (in both cases) by a SIE and then by adding an external shear term (which we will in the following denote by SIE_γ) and/or a SIS term to take into account the influence of the group in which the galaxy is embedded. Moreover, we add one or two substructures to take into account the effects on small scales. For PG1115+080 we use data in H band (see Table 1) taken from Impey et al. (1998), and for B1555+375 the data in the 5 GHz radio band (see Table 6) from Marlow et al. (1999). We allowed a conservative 1 σ error in the relative x- and y- positions of the image components (corresponding to an error of at most 5 mas), and 1 σ error on the values of the fluxes (corresponding to a variation by 20%). In each model we have different parameters and constraints, and the goodness of the fit is given by the χ^2 value, evaluated on the image plane (χ^2_{img}), and is a sum of different contributions: image positions and fluxes, and main galaxy position [5].

[4] The software is available via the web site: http://cfa-www.harvard.edu/castles

[5] There is an alternate way to define the χ^2 that is evaluated in the *source plane* (χ^2_{src}) (e.g., Kayser et al. 1990), which is an approximate version of χ^2_{img}: when using the minimization within this approximation the formation of additional images is not excluded, maybe yielding to a not realistic model. However, the approximation inherent χ^2_{src}, should properly be used only if a good model is already known, not in an initial search for a good model (Keeton 2001).

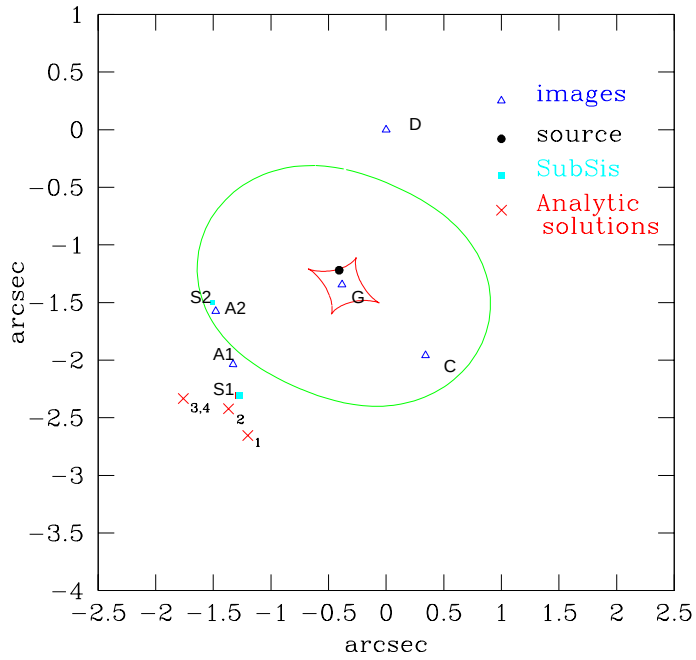

Fig. 1. PG1115+080: images, source and galaxy (G) positions are shown assuming a SIE_γ+SIS model. The position of the substructure for both models is also given: note that S1 is closer to the A1 image, while S2 to A2. The critical curve and the caustic are for the SIE_γ model without the modifications induced by the substructure. The analytic solutions as discussed in the Appendix are also shown. The solutions labeled as 3 and 4 are so close that on the figure they coincide.

4.1 PG1115+080

We model the main lens galaxy as a SIE and take into account the contribution due to the group of which the galaxy is part of either by adding a SIS_{group} component (Keeton 2003, Chen et al. 2003) or an external shear term. We consider both models to which we add one substructure described as a small SIS.

The results for PG1115+080, modeled as a SIE and an external shear or a SIS, are given in Tables 2, 3 and 4 (in the following we indicate with M the mass inside the Einstein radius) and in Fig. 1. In both cases we find good agreement with previous results (Impey et al. 1998, Chiba 2002). In the case SIE_γ we find for the external shear γ=0.11 and for its direction an angle of $\phi = 56^0$, which agree well with the results of Chiba (2002).

In a further step we add one substructure, using as starting parameters for its position and mass the analytic results as determined following the method

outlined in the previous section [6]. In the model $SIE_\gamma + SIS$ we have 11 parameters, i.e. for the main galaxy : Einstein radius (i.e. mass), ellipticity e and orientation PA, shear γ and its direction ϕ; for the substructure: the Einstein radius, position (corresponding to 2 parameters) and, moreover, the source position (2 parameters) and its flux. The observational constraints are 12, namely the 4 x 2 image positions and 4 fluxes.

In the model SIE+SIS$_{group}$+SIS, in which the group is modeled by a SIS, the substructure (denoted in Fig.1 by S2) is close to A2, whereas for the previous model it is close to A1 (denoted as S1 in Fig. 1). By adding one substructure the value of the anomalous flux ratio improves substantially for both models: getting lowered from 0.91 to 0.69 for the first model and to 0.66 for the second model, with χ^2_{tot}=1.3 and ≈ 0.4, respectively, which is quite good. [7]

The results from the simulations agree, as expected, quite well with the analytical ones. Since the mass of the substructures is very small as compared to the mass of the lens galaxy, the approximation used in the analytical approach to neglect the influence induced on the positions of the images by the substructures is quite well fulfilled. We checked this, indeed, on the results obtained from the numerical simulations.

Since the positions and magnifications of the images are only known within a certain accuracy, we computed the corresponding 1σ and 2σ ranges for the value of the mass of the substructure. Starting from our best model we consider two approaches. In the first we let all parameters (i.e. the main galaxy ones and the position of the substructure) vary, whereas in the second one we keep the main galaxy parameters fixed at the values given by the best fit model and let the remaining parameters vary. The high values for the total χ^2 are due to the bad galaxy position fit (in the first case) and to the bad image position fit (in the second case). In Fig. 2 we report χ^2 as a function of the substructure Einstein radius for the SIE+SIS$_{group}$+SIS model for both cases mentioned above. We do not consider larger values for the Einstein radius as this would correspond to masses for the substructure of order $M(< R_E) \approx 10^9 - 10^{10} M_\odot$, too big to be realistic and for which one would see effects on the image position or even image splitting. On the other hand we can also exclude Einstein radius that are too small. In fact, if it is true that with a standard accretion disk model we get a source size radius $R_s \approx 10^{15} cm$ (Chiba et al 2005) and that for the PG1115+080 system the real source size should be about 10-100 times

[6] Moreover, since we don't know a priori the source flux, we take the value we get from the SIE_γ model and, considering the observational fluxes with respect to the A1 image, we use them as starting values in the analytical system.

[7] By further adding a second substructure to the first model, we find even a lower value for the flux ratio, however, χ^2_{tot} and χ^2_{flux} increase, which indicates that this model does not correspond to a global minimum, but rather to a local minimum of the χ^2_{tot} surface.

Parameter	SIE_γ	$SIE+SIS_{group}$	SIE_γ+SIS	$SIE+SIS_{group}$+SIS
$R_{E,gal}$	1.03	1.14	1.12	1.03
$M_{gal}(M_\odot)$	1.23×10^{11}	1.05×10^{11}	1.24×10^{11}	1.05×10^{11}
$R_{E,group}$	–	2.30	–	2.11
M_{group} $(M_\odot)$	–	4.10×10^{11}	–	4.0×10^{11}
$R_{E,sub1}$	–	–	0.033	0.001
$M_{sub1}(M_\odot)$	–	–	1.00×10^{8}	1.00×10^{5}
$\sigma_v^{SIE}(kms^{-1})$	232.3	245.4	243.5	232.3
$\sigma_v^{SIS}(kms^{-1})$	–	–	39.2	6.8
A2/A1	0.91	0.95	0.69	0.66
γ	0.11	–	0.11	–
ϕ	56^0	–	56^0	–
χ^2	77	3.9	1.30	0.08

Table 2
PG1115+080: Parameters for different models, with and without substructure. γ and ϕ are the values of the external shear and its direction. R_E is expressed in arcsec (1 arcsec = 3.19 kpc h^{-1}). The 1D velocity dispersions for the main component and substructures are also reported. By adding a substructure the agreement between predicted and observed fluxes increases substantially.

Model	Image	κ	γ	μ	A2/A1
SIE_γ	A1	0.498	0.421	13.35	0.91
	A2	0.535	0.545	-12.17	–
$SIE+SIS_{group}$	A1	0.534	0.411	20.21	0.95
	A2	0.551	0.504	-19.31	–
SIE_γ+SIS	A1	0.554	0.372	16.54	0.69
	A2	0.561	0.531	-11.54	–
$SIE+SIS_{group}$+SIS	A1	0.531	0.410	19.46	0.66
	A2	0.565	0.517	-12.83	–

Table 3
PG1115+080: Values of shear, convergence and amplification for A1 and A2 images from simulations for the considered models.

Object	x (arcsec)	y (arcsec)	e	PA
Galaxy	-0.381	-1.345	0.14	-84^0
A1	-1.328	-2.037	–	–
A2	-1.478	-1.576	–	–
Sub1	-1.33	-2.20	–	–
Sub2	-1.52	-1.57	–	–

Table 4
PG1115+080: positions of the lens galaxy center, the close pair A1 and A2, as well as the substructure with respect to the C image (see Fig.1). Also ellipticity e and orientation PA of the semi major axis with respect to x-axis (as measured from East to North and centered in the C image) are given. The distances between the substructure and the images A1 and A2 are bigger than twice their corresponding Einstein radius. Thus no further images will be formed.

bigger (Pooley et al 2006), we can estimate roughly the limit of the Einstein radius for which the effects on the images become negligible. For a stellar $R_E \approx 10^{-5}$ arcsecs, that corresponds to 0.03 pc (on the lens plane), there would be no (or little) effect on an image of a source with $R_S \approx 0.1$ pc. The minimum value of the curve corresponds to an Einstein radius ≈ 0.001 arcsec. Anyway, the curve within the 2σ range is rather constrained (in both cases), leading thus in practice to a small degeneracy, with a rather narrow range for acceptable values of the substructure mass. The 2σ range is within an Einstein radius of 0.0005 and ≈ 0.005 arcsec corresponding to $\sim 2.5 \times 10^4\ M_\odot$ and $\sim 2.5 \times 10^6\ M_\odot$.

The 2σ range for the $SIE_\gamma + SIS$ model is somewhat larger. Considering for example the first case, the Einstein radius for the substructure could be as high as 0.1 arcsecs, leading to quite a big mass ($\approx 10^9 M_\odot$).

4.2 B1555+375

B1555+375 is another lens system for which the agreement between observations and model can be improved. Already by adding an external shear one can quite substantially improve the flux fitting, assuming for the lens galaxy a SIE model. Anyway, Dobler & Keeton (2006) consider this model unphysical (since ellipticity and shear turn out to be almost perpendicular) and discuss other models, adding substructures and giving lower limits on their masses. They find an acceptable model using two substructures in front of B and C images, respectively. Adding one substructure to the model SIE_γ does not

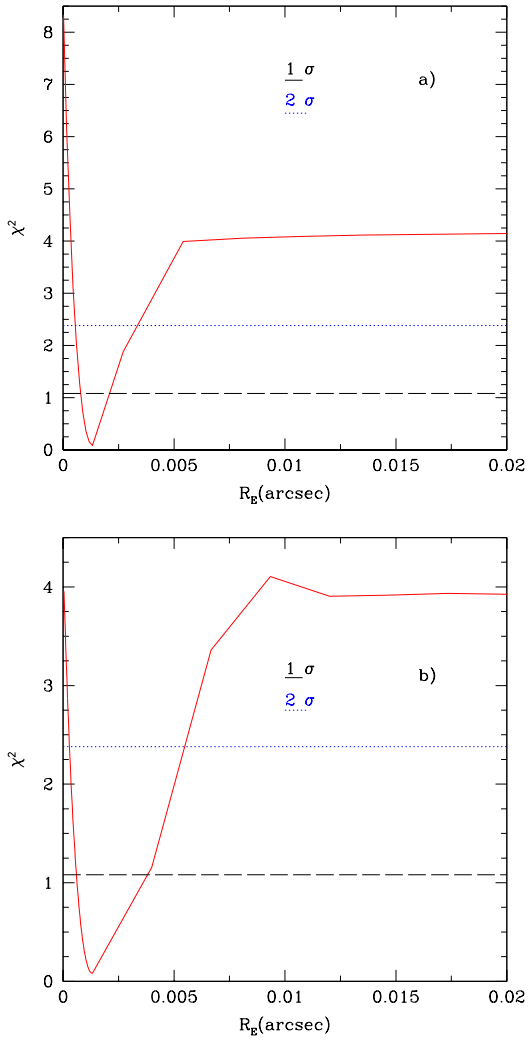

Fig. 2. 1σ and 2σ limits for the Einstein radius for the model SIE+SIS$_{group}$+SIS: a): letting all parameters fixed but the position of the subclump; b): letting all parameters vary.

improve the fit further [8] . On the other hand, adding two substructures (modeled as SIS with comparable masses and located near the pair of images due to the fold) to the simple SIE model, we get a value for the flux ratio B/A of 0.59, which is only slightly higher then the observed one of 0.57 The results are reported in Tables 6, 7 and 8 and in Fig. 3. For the model of a SIE_γ we get $\chi^2 = 1.29$ and $\chi^2_{flux} = 0.35$. For the solution with two substructures we find a $\chi^2 \approx 5$, with $N_{dof} = 5$.

As we pointed out above, in the radio band up to now the only successful

[8] We tried, as in the previous case, also analytically to estimate mass and position for a single SIS added to a SIE model, but the system of equations does not have in this case real solutions.

Image	x (arcsec)	y (arcsec)	S_5 (mJy)
A	0.0±0.005	0.0±0.005	17.0
B	-0.073±0.005	0.048±0.005	9.7
C	-0.411±0.005	-0.028±0.005	8.3
D	-0.162±0.005	-0.368±0.005	1.3

Table 5
B1555+375: Positions and photometric data of the 4 images as given by CLASS (from Marlow et al. 1999).

explanation for the flux anomalies is to consider substructures. Moreover, we notice that the SIE model does neither fit very well the fluxes of the other images besides the close pair ones.

As mentioned in the SIE_γ model we get a rather high value for the ellipticity (0.85) and for the external shear (0.23): such a strong shear can be induced by a group of galaxies located around the main lens. One has also to consider possible effects due to groups of galaxies which lie on the line-of-sight, both in the foreground and in the background (Williams et al. 2006). Other systems (like B1608+656 or HST 12531-2914) show such a high value for the external shear (see Witt & Mao 1997). In particular, B0128+437 seems to be quite similar to B1555+375 (see Philipps et al. 1999). Anyway, there are still not enough observations neither about the main galaxy nor about its environment, so that it is not possible to choose among the different solutions. However, our solution with two substructures involves a SIE lens model with an angular structure which is in agreement with previous works (Marlow et al. 1999 and Keeton, Gaudi & Petters 2005). Also for this model we computed the confidence intervals for the various parameters. As an example in Fig. 4 we show the contour ellipses for the confidence intervals of the Einstein radii of the substructures as obtained fixing the main galaxy parameters.

5 Discussion

We have analyzed two lens systems, PG1115+080 and B1555+375, which show an anomalous flux ratio for the two images near the critical curve, due to a fold configuration. These systems cannot be modeled using only smooth lens models like SIE, although they fit well all the positions of the images. We added one or two substructures, taking as starting parameters for our numerical simulations the ones obtained by an approximated analytical treatment.

In this way we reproduce well, in addition to the positions, also the fluxes

Parameter	SIE	SIE_γ	SIE+2SIS
$R_{E,gal}$	0.22	0.165	0.21
M_{gal} $(M_\odot)$	0.50	0.45	0.50×10^{10}
$R_{E,sub1}$	–	–	0.009
$R_{E,sub2}$	–	–	0.012
$M_{sub1}(M_\odot)$	–	–	8.1×10^6
$M_{sub2}(M_\odot)$	–	–	1.4×10^7
$\sigma_v^{SIE}(kms^{-1})$	170.1	147.3	165.6
$\sigma_v^{sub1}(kms^{-1})$	–	–	23.3
$\sigma_v^{sub2}(kms^{-1})$	–	–	24.7
B/A	0.93	0.61	0.59
e	0.53	0.85	0.53
PA	-2.42^0	-6.39^0	0.41^0
γ	–	0.23	–
ϕ	–	-78^0	–
χ^2	13.9	1.9	5.2

Table 6
B1555+375: Results from the simulations for two models without substructures and one model with two substructures. (Notice that for the latter model the χ^2 is higher, see text). The Einstein radii are expressed in arcsec. The system is well fitted already by adding external shear.

Object	x (arcsec)	y (arcsec)	e	PA
Lens	-0.162	-0.246	0.53	0.75^0
A	0.0	0.0	–	–
B	-0.075	0.043	–	–
Sub1	-0.060	0.094	–	
Sub2	0.101	0.001	–	

Table 7
B1555+375: Parameters of the lens model and of the added substructures. e and PA are ellipticity and orientation of the semi major axis with respect to x-axis (as measured from East to North and centered in the A image).

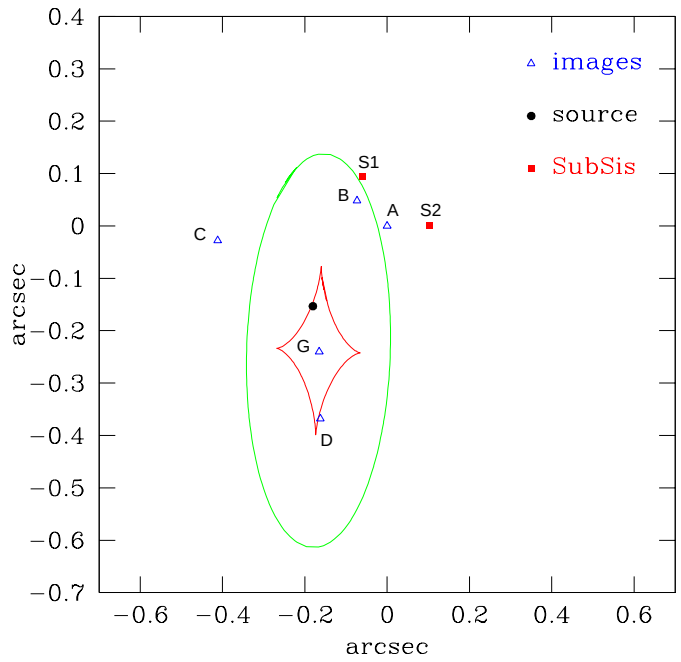

Fig. 3. B1555+375: images, source and galaxy (G) positions are shown assuming a SIE+2SIS model. The positions of the two substructures are also given. The critical curve and the caustic are for the SIE model alone without the modifications induced by the two substructures.

of the pair of images near the critical curve. In the PG1115+080 case we get a ratio of 0.69 as compared to the observed one of 0.65 if we consider a model SIE_γ + SIS or 0.66 for a model SIE+SIS_{group}+SIS and for B1555+375 a ratio of 0.59 instead of 0.57 with a SIE+2SIS model. We point out that for PG1115+080 when we consider the model SIE+SIS_{group}+ SIS we find that the substructure needed to explain the anomaly in the optical band lies close to the A2 image and has a mass $\approx 10^5 M_\odot$. On the other hand, the model SIE_γ requires a mass $\approx 10^8 M_\odot$ close to the A1 image that could in principle affect also larger λ bands, for which no anomaly has been reported yet (Chiba et al 2005). Therefore, this latter model is certainly less plausible if not already excluded. Clearly, new observations are still needed to better constrain the models.

In the case of B1555+375 we also explored simpler models (i.e. SIE, SIE plus simple external shear, or SIE + SIS) but we did not find any acceptable solution. We note that our best model is similar to the one found by Dobler & Keeton 2006: in their analysis, they concluded that the system B1555+375 has *two anomalous images*. Their approach is different, since they try to identify anomalies by relaxing the flux constraints on an image and fit all the others, image positions and fluxes. When a good model is found, they than conclude

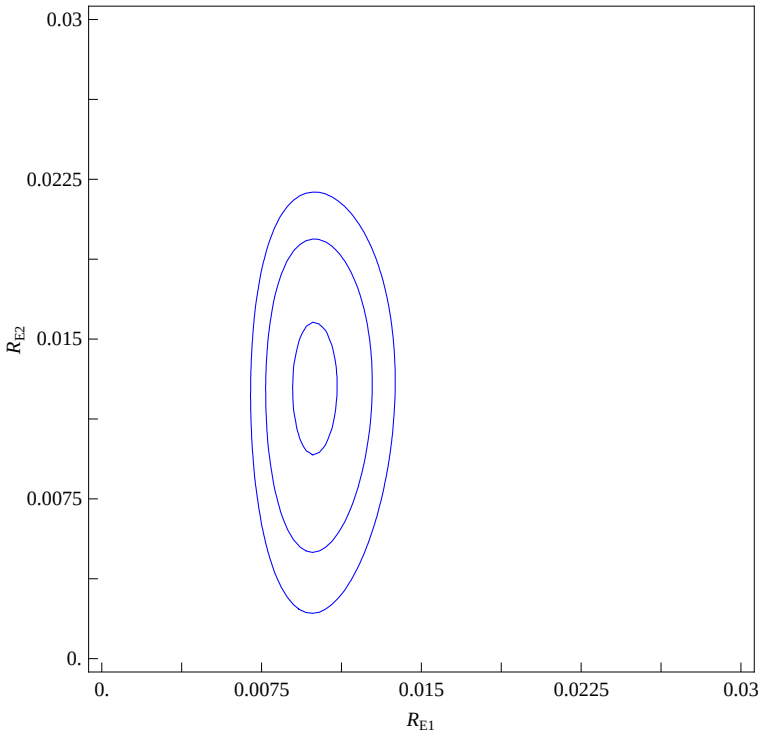

Fig. 4. B1555+375: Contour plot for the $1, 2$ and 3σ confidence intervals for the Einstein radii (in arcsec) of the substructures.

that the unconstrained image is anomalous and give a lower mass limit on the subclump likely responsible for the anomalous flux by optimizing χ^2 as a function of the subhalo Einstein radius and the source size. Nevertheless, they also need two substructures close to two different images (either in front of images A and C or close to images B and C) to fit the fluxes. Despite the fact that one of their models has $N_{dof} = 0$, the values of the subhalo masses are similar to ours (e.g. $\sim 10^{5-6} M_{\odot}$ within the Einstein radius). Finally, we would like to point out that the current observations towards B1555+375 seem not to reveal any nearby group to which the lens system belongs, so a SIE model plus external shear might be inadequate to describe the effect due to substructures, which are rather better modeled by a SIS.

In both cases the best models are the ones with additional substructures. Previously, the best models gave values for the anomalous flux ratio of 0.91 for PG1115+080 and 0.93 for B1555+375, respectively. The improvement achieved by just adding substructures is remarkable.

Our approach, although leading to better values for the anomalous flux ratios, is not completely new and indeed, as mentioned in the introduction previous works attempted to solve the anomalous flux ratios problem by adding perturbations until a good model was found. In particular, Keeton 2003, Inoue & Chiba 2005 studied the effect of substructures, modeled as SIS, in a convergence and shear field describing the main lens galaxy (or galaxies along

the line of sight, e.g. Keeton 2003). Mao & Schneider 1998, Metcalf & Madau 2001, Keeton 2001 analysed the problem by directly adding subclumps, in form of point masses, SIS, or plane-wave perturbations, in order to explain the observed anomalies. Chen 2003, Metcalf 2005, Keeton et al. 2005, Macciò & Miranda 2006 (and references therein) studied the problem by using statistical approaches and numerical simulations.

The masses of the substructures are in the range $\approx 10^5 - 10^8\ M_\odot$, and distant enough from the images not to induce the formation of additional ones. Given the mass range the perturbers could be globular clusters or small satellite galaxies, but also CDM dark substructures. In order to compare the masses we obtained with dark substructures as predicted by CDM, we notice that our values correspond to the mass enclosed within the Einstein radius, while CDM subhalo masses are defined as the mass enclosed within the tidal radius, which is usually much larger than R_E. However, without going too much into details, it is still possible to get a rough estimate of the mass within the tidal radius by calculating the 1D velocity dispersion of the subhalos from their Einstein radius and then by considering the $M \propto v_c^3$ (with the approximation $v_c = \sigma_v/\sqrt{3}$) relation found in numerical simulations (Bullock et al. 2001, Diemand et al 2004). Althought current simulations achieve a lower limit for CDM subhalo masses of $M \approx 10^{10-11} M_\odot$, we assume this relation to hold for lower values of the velocity dispersion and of the masses. Clearly, the extrapolation to lower velocities could suffer from resolution effects and numerical noise. In the system PG115+080 for the $SIE_\gamma + SIS$ model the substructure has a $\sigma_v \approx 39 km/s$, which leads to a mass of $\sim 7 \times 10^8 M_\odot$ (the mass within the Einstein radius, as given in Table 2, is instead $1 \times 10^8 M_\odot$), while in the model $SIE + SIS_{group} + SIS$ the substructure has $\sigma_v \approx 6.8 km/s$ corresponding to $\sim 4 \times 10^6 M_\odot$ (instead of $1 \times 10^5 M_\odot$). In the system B1555+375 the substructures have $\sigma_{v1} \approx 23\ km/s$ and $\sigma_{v2} \approx 25\ km/s$ respectively, which leads for both a corresponding mass of about $10^8 M_\odot$ (whereas, as given in Table 6, the mass within the Einstein radius is $\approx 10^7 M_\odot$). We roughly find that the mass within the tidal radius is about 10 times bigger than the one within the Einstein radius.

To get a rough estimate of the number of substructures expected to lie close to the images we follow the work of Diemand et al. (2004). They compute the two dimensional radial number density of subhalos inside a galaxy virial radius, from which it is then possible to get an estimate of the number of substructures inside a small area surrounding an image in a lens system. The number of subhalos with a mass greater than m inside an area A at a distance r from the center of the galaxy is given by (Macciò & Miranda 2006)

$$N_A(> m, r) = \frac{\langle N_{r_v}(> m_0)\rangle \frac{m_0}{m} N(r) A}{\pi r_v^2}\ , \tag{16}$$

where $\langle N_{r_v}(> m_0)\rangle$ is the average number of subhalos with $m > m_0$ inside the virial radius r_v of the galaxy and $N(r)$ describes the radial dependence of the number of substructures. The cumulative mass function of subhalos within the virial radius of an halo scales as $\propto m^{-1}$.

As an example for PG1115+080, we consider $m \geq 10^5 M_\odot$, ($m_0 \approx 10^7$) and a distance of the images from the center $r \approx 1.5$ arcsec ($N(r) \approx 2-6$, $\langle N_{r_v}(> m_0)\rangle \approx 166, r_{vir} = 268\ kpc$, see simulations G0 and G1 in table 1 of Diemand et al. 2004 and Macciò & Miranda 2006). Typically, a substructure is expected to lie at a distance from an image comparable to the separation between the close pair, which is about ≈ 0.5 arcsec. We, therefore, consider an area corresponding to a small disc with a radius about twice the separation distance, thus ≈ 1.0 arcsec (corresponding at $z_l = 0.31$ to A$\approx \pi(4.5)^2 kpc^2$). With these assumptions we expect 10 to 30 substructures in the considered area. If instead we require $m \geq 10^6 M_\odot$ then we find about 1 to 3 substructures, and 0.1 to 0.3 for $m \geq 10^7 M_\odot$. From these considerations we see that the expected number of substructures within the CDM model seems, in particular, to be lower than required when considering the model with a $10^8 M_\odot$ mass subclump or even bigger, whereas for models with a $10^6 M_\odot$ mass subclump it might be in better agreement.

For B1555+375 the above considerations apply as well: at $z_l = 0.5$, 1.0 arcsec= 6.114 *kpc*, thus the area around the image pair is A$\approx \pi(6.114)^2 kpc^2$. By using the same values as in the previous case the expected number of CDM subhalos bigger then 10^8 being close to the image pair is between 0.02 and ~ 0.1. Clearly, given the rough approximation used, some of them depending on extrapolations of numerical simulations of limited resolution, it is not possible to draw firm conclusions.

It is obviously also not possible to distinguish between different models, moreover it could be that some of the substructures are actually located along the line of sight rather than being in the surroundings of the lens galaxy. To this respect it is interesting to notice that with future ALMA observations one could solve this latter problem as pointed out by Inoue & Chiba (2005). They proposed a method to realize a 3D mapping of CDM substructures in extragalactic halos, based on astrometric shift measurements (at submillimeter wavelengths) of perturbed multiple images with respect to unperturbed images, with which it should be possible to break the degeneracy between the subhalo mass and a position along the line of sight to the image.

Also other explanations of the flux anomaly in multiple QSOlens systems have been considered in the literature, however the best solution, seems to be the presence of substructures in the halo of the lens galaxy.

For the second case (B1555+375) there are two acceptable solutions: with and

without any substructure. Even if a high shear value seems unplausible, we cannot yet rule out this possibility. A recent work (Williams et al. 2006) shows the importance of galaxy groups along the line of sight that can significantly impact the lens model. High-resolution VLA radio observations could help to constrain the lens model further. On the other hand, starting from the simple SIE model, we find a real good fit for the image positions and fluxes, if we add two substructures, still keeping acceptable values for the main lens parameters (in agreement with Marlow et al. 1999). We note also that for the B1555+375 system we assumed the redshifts of the source and the lens to be known. Even if these values might not be exact the uncertainties do not change the result significantly. For instance, if we let the redshifts ($z_s = 1.5$ and $z_l = 0.5$) vary by ± 0.3 and use a source redshift of $z_s = 1.8$ with $z_l = 0.2$ we get a mass for the first substructure of $3.3 \times 10^6 M_\odot (< R_E)$. By considering instead $z_s = 1.2$ and $z_l = 0.8$ the mass is $2.7 \times 10^7 M_\odot (< R_E)$. All other combinations will give a mass value within this range, and similarly for the second substructure.

Finally, we observe that the PG1115+080 system is radio-quiet, so that the microlensing hypothesis can not be ruled out (Pooley et al. 2006). However, given the different observations at the various wavelengths it might also be possible that both microlensing and millilensing are at work. A more accurate analysis about the source size could cast some light in constraining the substructure size. Since there are discussions about it, more high resolution observations are needed to definitely rule out the millilensing or microlensing hypothesis. On the other hand, for the B1555+375 system anomalies are evident in the available radio data, for which the most plausible explanation are CDM substructures in galactic halos.

Acknowledgments

We thank A. Macciò and M. Sereno for useful discussions. We also thank the referee for useful comments that improved the paper. Marco Miranda was partially supported by the Swiss National Science Foundation.

A Analytic estimates for convergence and shear due a substructure

We briefly present here the formalism used for the analytical approximation of the total convergence κ_{tot} and the total shear γ_{tot} in the presence of one perturber, located in the main lens plane. At each point of the lens plane we can evaluate the total amplification using the quantities:

	R_E	x	y
	arcsec	arcsec	arcsec
1	0.030	-1.199	-2.65
2	0.035	-1.825	-2.352
3	0.049	-1.363	-2.421
4	0.050	-1.76	-2.332

Table A.1
Analytic solutions for PG1115+080 as discussed in the text.

$$\kappa_{tot} = \kappa_{sie} + \Delta\kappa, \tag{A.1}$$
$$\gamma_{1tot} = \gamma_{1sie} + \Delta\gamma_1, \tag{A.2}$$
$$\gamma_{2tot} = \gamma_{2sie} + \Delta\gamma_2, \tag{A.3}$$
$$\mu^{-1} = (1-\kappa_{tot})^2 - \left[(\gamma_{1tot})^2 + (\gamma_{2tot})^2\right]. \tag{A.4}$$

κ_{sie} is the convergence due to the main lens and $\Delta\kappa$ is due to the perturber and similarly for the shear γ_{sie} and $\Delta\gamma$ (see Sec. 3.2). Dealing with a SIE model allows us to write (see Kormann et al. 1994):

$$\kappa_{sie} = \frac{R_{sie}}{2\sqrt{(\frac{2q^2}{1+q^2})(x_{sie}-x_P)^2 + (y_{sie}-y_P)^2}}, \tag{A.5}$$

Where q is the axis ratio of the elliptical model used for the galaxy acting as lens. The values for κ_{sie}, γ_{1sie} and γ_{2sie} are taken, for instance in the PG1115+080 case, from the SIE_γ model (which corresponds to the zero order approximation), computed in A1 and A2 (see Table 3) as well as the magnification factors with respect to the image A1 (and keeping the source flux as obtained from SIE_γ model). In this way the system

$$\begin{cases} \mu_{A1}^{-1} = (1-\kappa_{totA1})^2 - [(\gamma_{1totA1})^2 + (\gamma_{2totA1})^2] \\ \mu_{A2}^{-1} = (1-\kappa_{totA2})^2 - [(\gamma_{1totA2})^2 + (\gamma_{2totA2})^2] \\ \mu_{B}^{-1} \ \ = (1-\kappa_{totB})^2 - [(\gamma_{1totB})^2 + (\gamma_{2totB})^2] \end{cases} \tag{A.6}$$

has only three unknown quantities, namely R_{sis} and the perturber position given by (x_{sis}, y_{sis}). Since the system is non-linear, we get different sets of solutions, some of which turn out to be unphysical. The allowed solutions are near the close pair (see Table A1). We marked their positions on Figure 1. We used then these solutions as input parameters for the numerical simulation. It turns out that all converge to the same model $SIE_\gamma + SIS$ discussed in Sect. 4.1.

References

[1] Amara, A., Metcalf, R.B., Cox, T.J., & Ostriker, J.P. 2006, MNRAS, 367, 1367

[2] Barkana R., 1997, ApJ, 489, 21

[3] Biggs A.D. et al., 2004, MNRAS, 350, 949

[4] Bradač M. et al., 2002, A&A, 388, 373

[5] Bullock, J. S., Kravtsov, A. V., & Weinberg, D. H. 2000, ApJ, 539, 517

[6] Bullock, J. S., Kolatt, T. S., Sigad, Y., Somerville, R. S., Kravtsov, A. V., Klypin, A. A., Primack, J. R., & Dekel, A. 2001, MNRAS, 321, 559

[7] Chang K., Refsdal S., 1979, Nature, 282, 561

[8] Chiba M., 2002, ApJ, 565, 71

[9] Chiba, M., Minezaki, T., Kashikawa, N., Kataza, H., Inoue, K.T., 2005, ApJ, 627, 53

Chiba M., 2002, ApJ, 565, 71

[10] Chen J., Kravtsov A.V., Keeton C.R., 2003, ApJ, 592, 24

[11] Congdon, A. B., & V Keeton, C. R. 2005, MNRAS, 364, 1459

[12] Courbin F. et al., 1997, A&A, 324, 1

[13] Dalal N., Kochanek C.S, 2002, ApJ, 572, 25

[14] Diemand J., Moore B., Stadel J., 2004, MNRAS, 352, 535

[15] Diemand, J., Kuhlen, M., & Madau, P. 2007, ApJ, 657, 262

[16] Dobler G, Keeton, C.R., 2006, MNRAS, 365, 1243

[17] Evans, N. W., & Witt, V H. J. 2003, MNRAS, 345, 1351

[18] Falco E.E., Lehár J., Shapiro I.I., 1997, AJ, 113, 540

[19] Fassnacht C.D., Lubin L.M., 2002, AJ, 123, 627

[20] Hege E. K., Hubbard E. N., Strittmatter P. A., Worden S. P., 1981, ApJ, 248, 1

[21] Impey C.D. et al., 1998, ApJ, 509, 551

[22] Inoue K.T., Chiba M., 2005, ApJ, 634, 77

[23] Jackson N. et al., 1998, MNRAS, 296, 483

[24] Kayser, R., Surdej, J., Condon, J. J., Kellermann, K. I., Magain, P., Remy, M., & Smette, A. 1990, ApJ, 364, 15

[25] Keeton C.R., 2001, astro-ph/0102340

[26] Keeton C. R., Kochanek C. S., 1997, ApJ, 487, 42

[27] Keeton C.R., Kochanek C.S., Seljak U., 1997, ApJ, 490, 493

[28] Keeton C.R., 2003, ApJ, 584, 664

[29] Keeton C.R., Scott Gaudi B., Petters A.O., 2005 ApJ, 635, 35

[30] Klypin A., Kravtsov A.V., Valenzuela O., Prada F., 1999, ApJ, 522, 82

[31] Kormann R., Schneider P., Bartelmann M., 1994, A&A, 284,285

[32] Kochanek C.S., Dalal N., 2004, ApJ, 610, 69

[33] Kochanek C.S., 2004, Part 2 of: Gravitational Lensing: Strong, Weak and Micro, Proceedings of the 33rd Saas-Fee Advanced Course, G. Meylan, P. Jetzer & P. North, eds. (Springer-Verlag: Berlin), astro-ph/0407232

[34] Kravtsov, A. V., Gnedin, O. Y., & Klypin, A. A. 2004, ApJ, 609, 482

[35] Kravtsov, A. V., Gnedin, O. Y., & Klypin, A. A. 2004, ApJ, 609, 482

[36] Macciò, A. V., Moore, B., Stadel, J., & Diemand, J. 2006, MNRAS, 366, 1529

[37] Macciò A.V., Miranda M., 2006, MNRAS, 368, 599

[38] Mao S., Schneider P., 1998, MNRAS, 295, 587

[39] Marlow D.R. et al., 1999, AJ, 118, 654

[40] Metcalf R.B., Madau P., 2001, ApJ, 563, 9

[41] Metcalf R.B., Zhao H., 2002, ApJ, 567, L5

[42] Metcalf, R. B., Moustakas, L. A., Bunker, A. J., & Parry, I. R. 2004, ApJ, 607, 43

[43] Metcalf R.B., 2005, ApJ, 622, 72

[44] Minezaki T. et al., 2004, ApJ, 600, L35

[45] Moore B., Quinn T., Governato F., Stadel J., Lake G. 1999, MNRAS, 310, 1147

[46] Moore, B., Diemand, J., Madau, P., Zemp, M., & Stadel, J. 2006, MNRAS, 368, 563

[47] Mortonson, M. J., Schechter, P. L., & Wambsganss, J. 2005, ApJ, 628, 594

[48] Narayan R., Schneider P. 1990, MNRAS, 243, 192

[49] Philipps P.M. et al., 2000, MNRAS, 319, L7

[50] Pooley, D., Blackburne, J.A., Rappaport, S., Schechter, P.L., & Fong, W.-f. 2006, ApJ, 648, 67

[51] Rauch, K. P., & Blandford, R. D. 1991, ApJ, 381, L39

[52] Read, J. I., Saha, P., & Maccio, A. V. 2007, ApJ, 667, 645

[53] Schechter P.L. et al., 1997, ApJ, 475, 85

[54] Schneider P., Ehlers J., Falco, E.E., 1992, Gravitational Lenses (Springer-Verlag) (SEF)

[55] Spergel, D. N., et al. 2003, ApJ, 148, 175

[56] Tonry, J. L. 1998, AJ, 115, 1

[57] Wambsganss, J., Schneider, P., & Paczyński, B. 1990, ApJ, 358, L33

[58] Wambsganss J., Paczyński B., 1994, AJ, 108, 1156

[59] Weymann R.J. et al., 1980, Nature, 285, 641

[60] Williams K. A., Momcheva I., Keeton, C.R., Zabludoff A.I., Lehar J., 2006, ApJ, 646, 85

[61] Witt Hans J., Mao Shude, 1997, MNRAS, 291, 211

[62] Wyithe, J. S. B., Webster, R. L., Turner, E. L., & Mortlock, D. J. 2000, MNRAS, 315, 62

[63] Young P. et al., 1981 ApJ, 244, 723

[64] Yoo J. et al., 2005, ApJ, 626, 51